Nanoscale Res Lett (2009) 4:1004–1008
DOI 10.1007/s11671-009-9353-3

NANO EXPRESS

Growth of Comb-like ZnO Nanostructures for Dye-sensitized Solar Cells Applications

Ahmad Umar

Received: 20 April 2009 / Accepted: 14 May 2009 / Published online: 29 May 2009

Abstract Dye-sensitized solar cells (DSSCs) were fabricated by using well-crystallized ZnO nanocombs directly grown onto the fluorine-doped tin oxide (FTO) via non-catalytic thermal evaporation process. The thin films of as-grown ZnO nanocombs were used as photoanode materials to fabricate the DSSCs, which exhibited an overall light to electricity conversion efficiency of 0.68% with a fill factor of 34%, short-circuit current of 3.14 mA/cm^2, and open-circuit voltage of 0.671 V. To the best of our knowledge, this is first report in which thin film of ZnO nanocombs was used as photoanode materials to fabricate the DSSCs.

Keywords ZnO · Nanocombs · Dye-sensitized solar cells · Structural and optical properties

Introduction

The II-VI semiconductor ZnO is one of the most important multifunctional materials due to its various exotic properties such as direct wide band gap (3.37 eV) and high optical gain of 300 cm^{-1} (100 cm^{-1} for GaN) at room temperature, large saturation velocity (3.2×10^7 cm/s), high breakdown voltage, large exciton binding energy (60 meV), piezoelectric, biocompatibility, and so on [1–12]. ZnO can be used in variety of high-technological practical applications such as ultraviolet (UV) lasers, light-emitting diodes, photodetectors, piezoelectric transducers and actuators, hydrogen storage, chemical and biosensors, surface acoustic wave guides, solar cells, photocatalysts, etc. [1–24]. Among various applications, the use of ZnO nanomaterials as photoelectrodes for the fabrication of dye-sensitized solar cells (DSSCs) has received a great attention due to its compatibility and higher electronic mobility with TiO_2 nanomaterials and similar electron affinity and band gap (3.37 eV at 298 K) [17]. Therefore, some ZnO nanostructures have been used as photoelectrode materials for the fabrication of DSSCs and reported in the literature [15–21]. Hsu et al. [15] reported the ZnO nanorods-based DSSC with the electricity conversion efficiency (ECE) of 0.22%. Branched ZnO nanowires based DSSCs, grown by thermal evaporation process at 800–1,000 °C, with an ECE of ~0.46% have been reported by Suh et al. [16]. In another report, by using branched ZnO nanowires grown by MOCVD process, the fabricated DSSCs exhibited an ECE of ~0.5% [24]. Cheng et al. [19] also demonstrated the thermally grown ZnO nanorods-based DSSC with the ECE of 0.6%.

In this paper, we report the direct synthesis of well-crystallized ZnO nanocombs on FTO substrates and their DSSCs application. To fabricate the DSSCs, the thin films of as-grown ZnO nanocombs on FTO substrates were used as photoanode materials, which exhibited an overall light to electricity conversion efficiency of 0.68%. To the best of our knowledge, the use of ZnO nanocombs for the fabrication of DSSCs is not reported yet in the literature.

Experimental Details

ZnO nanocombs were grown in a horizontal quartz tube furnace on the FTO substrate. The high purity metallic zinc powder (99.999%) and oxygen gas were used as source

A. Umar (✉)
Department of Chemistry, Faculty of Science, Advanced Materials and Nano-Engineering Laboratory (AMNEL), Najran University, P.O. Box 1988, Najran 11001, Kingdom of Saudi Arabia
e-mail: umahmad@nu.edu.sa

materials. In a typical reaction process, about 1.5 g of metallic zinc powder was put into a ceramic boat and placed at the center of the quartz tube. The furnace temperature was raised up to the desired temperature, and oxygen and nitrogen were fed continuously into the quartz tube furnace with the flow rates of 60 and 240 sccm, respectively. The temperature of the substrate, placed 8-cm away from the source boat, was 570 °C. The reaction lasted for 60 min. During this period, the metallic zinc was vaporized and oxidized with O_2, and finally deposited onto the FTO substrate.

For DSSC fabrication, the prepared ZnO nanocomb thin-film electrodes was immersed in the ethanolic solution of 0.3 mM cis-bis (isothiocyanato) bis(2,2′-bipyridyl-4, 4′-dicarboxylato)-ruthenium (II) bis-tetrabutylammonium (N719, Solaronix) at room temperature for 6 h. The dye-adsorbed ZnO nanocombs thin-film electrodes were then rinsed with acetonitrile and dried under a nitrogen stream. Pt counter electrode was prepared by electron beam deposition of a thin layer of Pt ($\sim$ 60 nm) on the top of ITO glass. The Pt electrode was placed over the dye-adsorbed ZnO nanocombs electrode, and the edges of the cell were sealed with 60-μm thick sealing sheet (SX 1170-60, Solaronix). Sealing was accomplished by pressing the two electrodes together on a double hot-plate at a temperature of about 70 °C. The electrolyte, consisting of 0.5 M LiI, 0.05 mM I_2, and 0.2 M tert-butyl pyridine in acetonitrile, was introduced into the cell through one of two small holes drilled in the counter-electrode. The holes were then covered and sealed with a small square of sealing sheet and microscope objective glass. The resulting cell had an active area of about 0.25 cm^2. Photocurrent–Voltage (I–V) curve was measured by using computerized digital multimeters. The light source was 1000-W metal halide lamp, and its radiant power was adjusted with respect to Si reference solar cell to about one-sun-light intensity (100 mW/cm^2).

Results and Discussion

Structural and Optical Properties of As-grown ZnO Nanocombs

Figure 1a shows the low-magnification FESEM image of the ZnO nanocombs and reveals that the nanocombs are densely grown and uniformly distributed over the large area of the substrate surface. From the high-magnification images, it is seen that the nanocombs are made by two components, i.e. nanorodlike branches and wide ribbonlike stems. The branches (teeth) of the nanocombs are uniform and nicely attached along one side of the ribbonlike stem. The width of the stem is $\sim 1.2 \pm 0.3$ μm, and the stem is several micrometers long. The diameter and length of each tooth is $\sim 300 \pm 100$ nm and $\sim 3 \pm 0.5$ μm respectively. These teeth are arranged in a proper manner with a distance of $\sim 200 \pm 50$ nm between each other [Figure (b) and inset (b)]. The X-ray diffraction (XRD) pattern exhibits

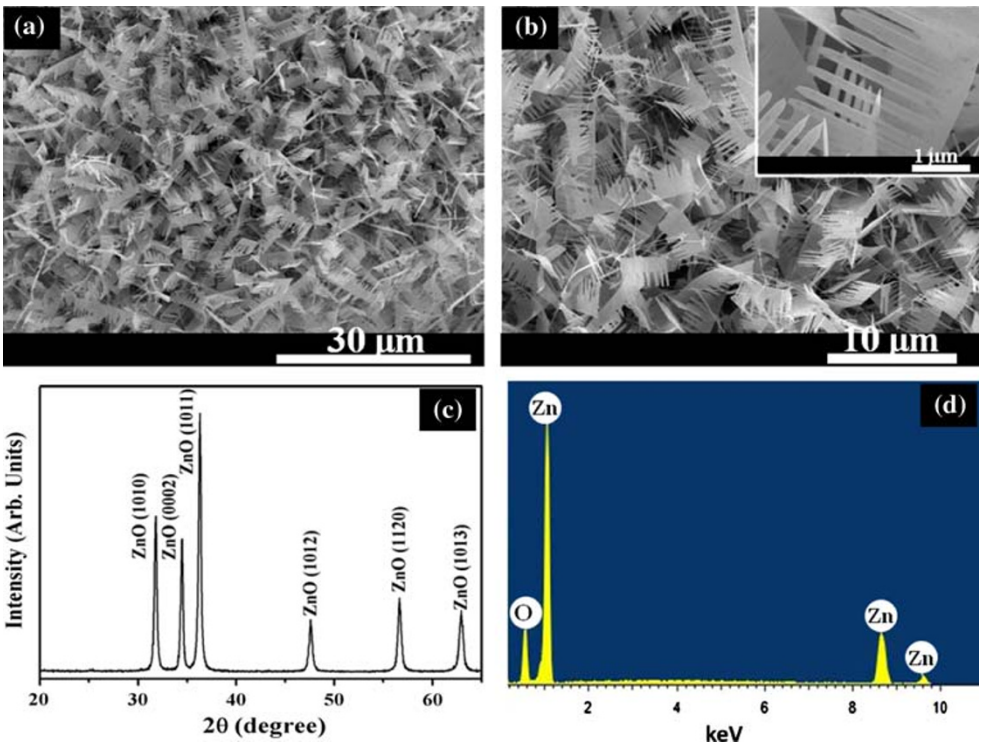

Fig. 1 Typical (**a**) low- and (**b**) high-magnification FESEM images; (**c**) XRD pattern and (**d**) EDS spectrum of high density-grown ZnO nanocombs on FTO substrate

that the as-grown nanocombs are single-crystalline with the wurtzite hexagonal-phase pure ZnO (JCPDS # 36–1451) (Fig. 1c). Except ZnO, no characteristic peaks for other impurities such as zinc and substrate were observed in the spectrum, which confirms that the obtained products are single-crystalline wurtzite hexagonal-phase ZnO grown in highdensity on the FTO substrate. In addition to this, the energy dispersive spectroscopy (EDS) confirmed that the as-grown nanocombs are made with almost 1:1 stoichiometry of zinc and oxygen (Fig. 1d). Further structural characterization of the grown products was made using the transmission electron microscope (TEM) and high-resolution TEM combined with the selected area electron diffraction (SAED) pattern. Figure 2a shows the low-magnification TEM image of the nanocombs, which reveals the full consistency with the FESEM observation in terms of morphology and dimensionality. Clearly, it is seen in the TEM image that the branches of the nanocombs are attached along one side of the ribbonlike stem. The HRTEM image of one tooth of comblike structure circled in figure(a) demonstrated a well-defined lattice fringes with the lattice spacing of 0.52 nm, corresponds to the *d*-spacing of the [0001] crystal plane of the wurtzite hexagonal ZnO, confirmed that the branches of the comb structures are grown along the [0001] direction (Fig. 2b). The corresponding SAED pattern of a branch of comb projected to the [2$\bar{1}\bar{1}$0] zone axis is also consistent with HRTEM observation (Fig. 2b, inset). Figure 2c shows the room-temperature photoluminescence (PL) spectrum measured using a He–Cd laser line with an exciton wavelength of 325 nm. The obtained PL spectrum exhibited a narrow peak at ~385 nm in the UV region, also called near band edge emission, and a broad emission peak at ~570 nm in the visible region, also known as deep-level emission. It is well known that the UV emission has been realized to the exciton emission, while the deep-level emission is generally explained as the radial recombination of photo-generated hole with a singly ionized charged state of the oxygen vacancy [22].

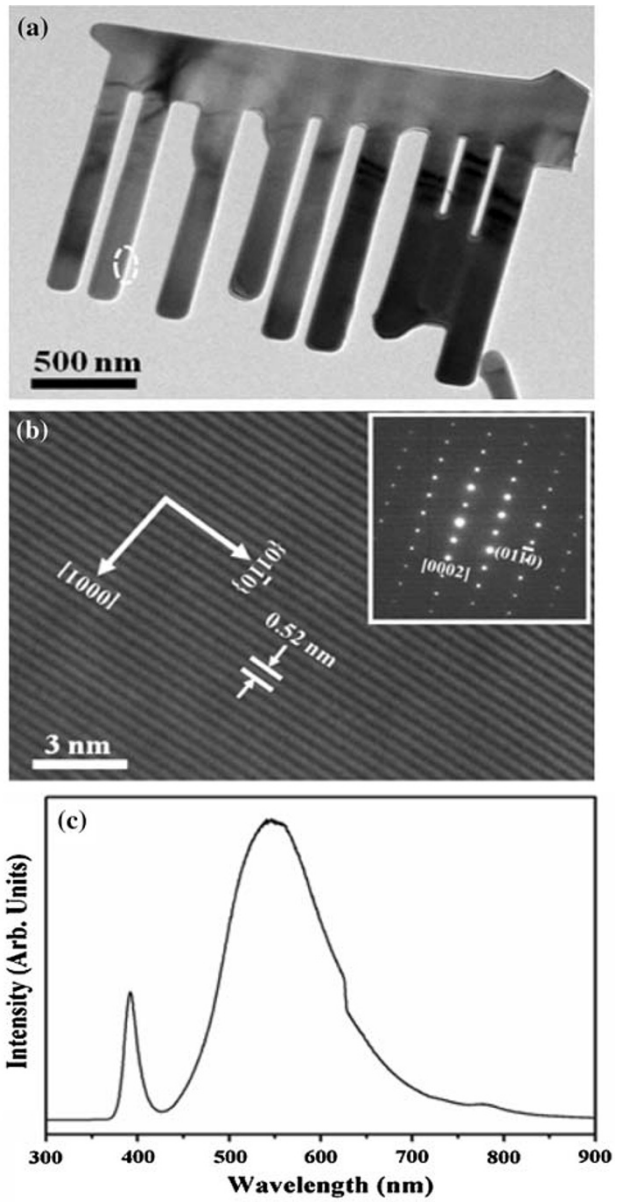

Fig. 2 Typical (**a**) low- and (**b**) high-magnification TEM image and their corresponding SAED pattern [*inset* (**b**)]; and (**c**) room-temperature PL spectrum of as-grown ZnO nanocombs used for the fabrication of DSSC

As a wurtzite hexagonal-phase ZnO possesses a positively charged Zn-(0001) surfaces that are catalytically active, the negatively charged O-(0001) surfaces are chemically inert [23]. The comb stem grows along the [2$\bar{1}$ $\bar{1}$0] direction, while the top and bottom surfaces are zinc and oxygen terminated (0001) respectively. It is reported that the catalytically active Zn-terminated (0001) surfaces tend to have tiny Zn clusters and other Zn particles at the growth front, which could provide an active site for the further growth process, and hence comb teeth can grow in front of zinc-terminated (0001) surfaces [23]. Due to higher growth velocity in [0001] direction of ZnO crystals, the comb teeth were also grown in [0001] directions [23].

Photovoltaic Properties of As-grown ZnO Nanocombs

Figure 3a shows the current density–voltage (I–V) characteristics for DSSCs fabricated with ZnO nanocombs thin-film electrodes and measured under a simulated illumination with a light intensity of 100 mW/cm^2 (AM = 1.5). A maximum electricity conversion efficiency of 0.68% was achieved by highly branched ZnO nanocombs thin-film DSSCs. The fabricated DSSCs also obtained a maximum short-circuit current density (J_{SC}) of 3.14 mA/cm^2 with low V_{OC} of 0.671 V and low FF of 34%. The low J_{SC} and

conversion efficiency reveal that low dye absorption on the surface of ZnO thin film and result in the low-light harvesting and fast interface recombination rate of electron and holes [24]. It is reported that the interface recombination loss in ZnO-based DSSCs is mostly due to the uncovered oxide surface (with no dye molecule anchored on), where oxide contacts with electrolyte closely and thus increases the probability of charge recombination between the electrons in oxide and the holes in the electrolyte [24]. The low V_{OC} can be explained by the gapping between the spikes of ZnO nanocombs, which also cause direct contact of electrolyte to the FTO glass, [21] results the low FF. The low FF and photocurrent may be explained by the fast recombination rate between the photoexcited carriers at the nanocombs and the electrolyte interfaces, which is related to series resistance $R_s = (dV/dI)_{I=0}$ [25]. Generally, R_s is ascribed to the bulk resistance of semiconductor oxide films, TCO electrode, metallic contacts, and electrolyte. From the *I–V* curve, R_s of ZnO nanocombs-based DSSC is relatively high ($\sim 213\ \Omega\ cm^2$), which increased the charge recombination between the photoexcited carriers at the nanocombs and the redox electrolyte. The high R_s results in the low FF and photocurrent. Figure 3b shows the UV–Vis absorption spectrum of desorbed dye obtained from the ZnO electrodes by dipping the ZnO nanocombs electrode in 0.1 mM NaOH solution for 10 min. It was observed that low dye absorption ($\sim 3.23 \times 10^{-8}$ mol/cm^2) by ZnO nanocombs film surface electrode was probably due to the nonporous morphologies of the nanocombs. It is well known that the high dye absorption by porous thin film leads to high light-harvesting efficiency [26]. Therefore, low J_{SC} and η are related to less absorption of dye molecules and insufficient light harvesting from the ZnO nanocombs thin-film electrodes. The inset of Fig. 3b demonstrates the general morphologies of ZnO nanocombs after the dye absorption and, interestingly, there was no distinct change observed in the general morphologies of the nanocombs after dye absorption, hence the nanocombs retain their morphologies after dye absorption.

In order to elucidate the charge transfer properties of as-grown ZnO nanocombs substrates, an electrochemical impedance spectroscopy (EIS) measurement was used. EIS measurements were taken out under the illumination of 100 mW/cm^2 (AM = 1.5) by applying a 10 mV Ac signal over the frequency range of 10 Hz–100 kHz using a potentiostat with lock in amplifier, as shown in Fig. 4. According to the diffusion–recombination model proposed by Bisquert et al. [27, 28], an equivalent circuit representing DSSCs was illustrated (inset of Fig. 4). Equivalent circuit is composed of the resistance of redox electrolyte solution (R_S), the charge transfer resistance at the interface of electrolyte and ZnO nanocombs (R_{CT}), the charge transfer resistance at the interface of ZnO nanocombs and

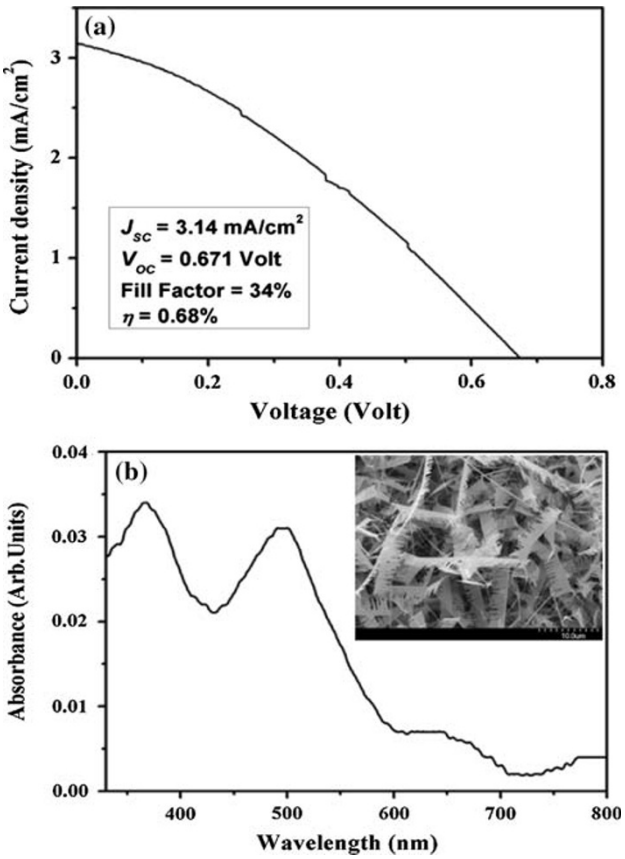

Fig. 3 **a** Current–voltage (J–V) characteristics of ZnO nanocombs-based DSSC and (**b**) typical UV–Vis absorption spectra of the desorbed dye (N719) from the ZnO nanocombs electrode thin films. Inset of (**b**) exhibits the surface morphology of the comblike structures after the desorption of dye

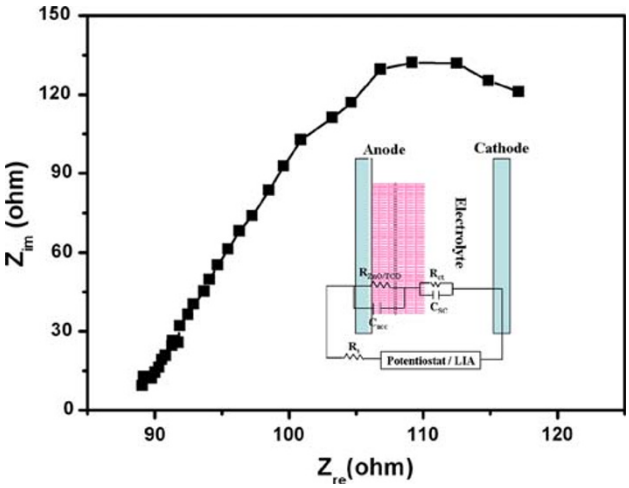

Fig. 4 Nyquist plots of the impedance data of ZnO nanocomb-based DSSCs. Inset shows the equivalent circuit model of the DSSCs, where R_s is the resistance of redox electrolyte solution, R_{CT} the charge transfer resistance at the interface of electrolyte and ZnO nanocombs, [R_{CT}] is the charge transfer resistance at the interface of ZnO nanocombs and TCO [$R_{ZnO/TCO}$], is the capacitance of accumulation (of e-) layer of the ZnO nanocombs [C_{ACC}] and C_{SC} space charge capacitance

TCO ($R_{ZnO/TCO}$), the capacitance of accumulation (of e-) layer of the ZnO nanocombs (C_{ACC}) and space charge capacitance (C_{SC}) [29]. The value of real impedance (Z_{re}) at high and medium frequencies represents the $R_{ZnO/TCO}$ and R_{CT}. Figure 4 exhibits the AC impedance curve of DSSC fabricated with thermally grown ZnO nanocombs electrode. A very high $R_{ZnO/TCO}$ (90 Ω) and R_{CT} (29.6 Ω) were obtained for ZnO nanocombs thin-film electrodes, which are lesser than that of TiO_2 thin-film electrodes [30]. It is reported that a small R_{CT} suggests fast electron transfer, whereas a large R_{CT} indicates slow electron transfer [31]. The high R_{CT} (29.6 Ω) of ZnO nanocombs thin-film electrode explains the slow electron transfer, which results in the low photocurrent density and conversion efficiency. Therefore, the high charge transfer resistance at ZnO/electrolyte interface reveals a slow electron transfer through the ZnO nanocombs thin-film electrode, which results in the low I_{SC}, FF, and conversion efficiency of the fabricated DSSC.

Conclusion

In summary, well-crystallized ZnO nanocombs were directly grown onto the FTO substrate via noncatalytic simple thermal evaporation process and utilized as photoanode materials to fabricate the DSSCs. The fabricated DSSCs demonstrated an overall light to electricity conversion efficiency of ~0.68% with a fill factor of 34%, short-circuit current of 3.14 mA/cm^2 and open-circuit voltage of 0.671 V. This research opens a new way to utilize various kinds of ZnO nanostructures as photoanode material for the fabrication of efficient DSSCs.

Acknowledgements This work has been done through the service contract between Najran University, Saudi Arabia and Chonbuk National University, South Korea. Author would like to thank Professor Yoon-Bong Hahn, School of Semiconductor and Chemical Engineering, Chonbuk National University and Dr. D. H. Kim, Hanyang University, South Korea for useful discussions and helps to carry out the experiments. This work was partially supported by the research project funded by Najran University, Najran, Saudi Arabia.

References

1. Ü. Özgür, Y.I. Alivov, C. Liu, A. Teke, M.A. Reshchikov, S. Dogan, V. Avrutin, S.-J. Cho, H. Morkoç, J. Appl. Phys. **98**, 41301 (2005). doi:10.1063/1.1992666
2. M.H. Huang, S. Mao, H. Feick, H.Q. Yan, Y. Wu, H. Kind, E. Weber, R. Russo, P. Yang, Science **292**, 1897 (2001). doi:10.1126/science.1060367
3. Z.L. Wang, Annu. Rev. Phys. Chem. **55**, 159 (2004). doi:10.1146/annurev.physchem.55.091602.094416
4. A. Umar, Y.B. Hahn, Cryst. Growth Des. **8**, 2741 (2008). doi:10.1021/cg700887z
5. A. Umar, S.H. Kim, B. Karunagaran, E.K. Suh, Y.B. Hahn, Inorg. Chem. **47**, 4088 (2008). doi:10.1021/ic701929p
6. J. Bao, M.A. Zimmler, F. Capasso, X. Wang, Z.F. Ren, Nano Lett. **6**, 1719 (2006). doi:10.1021/nl061080t
7. A. Umar, S.H. Kim, H. Lee, N. Lee, Y.B. Hahn, J. Phys. D Appl. Phys. **41**, 065412 (2008). doi:10.1088/0022-3727/41/6/065412
8. A. Umar, M.M. Rahman, S.H. Kim, Y.B. Hahn, Chem. Commun. (Camb). **2**, 166 (2008). doi:10.1039/b711215g
9. X.D. Wang, J.H. Song, J. Liu, Z.L. Wang, Science **316**, 102 (2007). doi:10.1126/science.1139366
10. Q. Wan, C.L. Liu, X.B. Yu, T.H. Wang, Appl. Phys. Lett. **84**, 124 (2009). (2004)
11. W. Wang, B. Zeng, J. Yang, B. Poudel, J.Y. Huang, M.J. Naughton, Z.F. Ren, Adv. Mater. **18**, 3275 (2006)
12. A. Umar, M. M. Rahman, A. Al-Hajry, Y.B. Hahn. Electrochem. Commun. 11:278. doi:10.1016/j.elecom.2008.10.037
13. A. Umar, M.M. Rahman, A. Al-Hajry, Y.B. Hahn, Talanta **78**, 284 (2009). doi:10.1016/j.talanta.2008.11.018
14. A. Umar, M.M. Rahman, M. Vaseem, Y.B. Hahn, Electrochem. Commun. **11**, 118 (2009). doi:10.1016/j.elecom.2008.10.046
15. Y.F. Hsu, Y.Y. Xi, A. Djurisic, W.K. Chen, Appl. Phys. Lett. **92**, 133507 (2008). doi:10.1063/1.2906370
16. D.I. Suh, S.Y. Lee, T.H. Kim, J.M. Chun, E.K. Suh, O.B. Yang, S.-K. Lee, Chem. Phys. Lett. **442**, 348 (2007). doi:10.1016/j.cplett.2007.05.093
17. C.H. Ku, J.J. Wu, Appl. Phys. Lett. **91**, 93117 (2007). doi:10.1063/1.2778454
18. C.Y. Jiang, X.W. Sun, G.Q. Lo, D.L. Kwong, J.X. Wong, Appl. Phys. Lett. **90**, 263501 (2007). doi:10.1063/1.2751588
19. A.J. Cheng, Y. Tzeng, Y. Zhou, M. Park, T. Wu, C. Shannon, D. Wang, W. Lee, Appl. Phys. Lett. **92**, 92113 (2008). doi:10.1063/1.2889502
20. Y. Gao, M. Nagai, T.C. Chang, J.J. Shyue, Cryst. Growth Des. **7**, 2467 (2007). doi:10.1021/cg060934k
21. A.D. Pasquier, H. Chen, Y. Lu, Appl. Phys. Lett. **89**, 253513 (2006). doi:10.1063/1.2420779
22. K. Vanheusden, C.H. Seager, W.L. Warren, D.R. Tallant, J.A. Voigt, J. Appl. Phys. **79**, 7983 (1996). doi:10.1063/1.362349
23. Y. Ding, X.Y. Kong, Z.L. Wang, Phys. Rev. B **70**, 235408 (2004). doi:10.1103/PhysRevB.70.235408
24. J.B. Baxter, E.S. Aydil, Appl. Phys. Lett. **86**, 53114 (2005). doi:10.1063/1.1861510
25. H. Chen, A.D. Pasquier, G. Saraf, J. Zhong, Y. Lu., Semicond. Sci. Technol. **23**, 045004 (2008). doi:10.1088/0268-1242/23/4/045004
26. E. Hosono, S. Fujihara, T. Kimura, Electrochim. Acta **49**, 2287 (2004). doi:10.1016/j.electacta.2004.01.009
27. J. Bisquert, G. Garcia-Belmonte, F. Fabregat-Santiago, N.S. Ferriols, P. Bogdanoff, E.C. Pereira, J. Phys. Chem. B **104**, 2287 (2000). doi:10.1021/jp993148h
28. F. Fabregat-Santiago, J. Bisquert, E. Palomares, L. Otero, D. Kuang, S.M. Zakeeruddin, M. Grätzel, J. Phys. Chem. C **111**, 6550 (2007). doi:10.1021/jp066178a
29. J.R. Macdonald, *Impedance spectroscopy* (Wiley, New York, 1987)
30. A. Hagfeldt, M. Grätzel, Acc. Chem. Res. **33**, 269 (2000). doi:10.1021/ar980112j
31. A.J. Brad, L.R. Faulkner, *Electrochemical methods: fundamentals and applications* (Wiley, New York, 1980), p. 350